


PAPER

Anti-impact behavior of a novel soft body armor based on shear thickening gel (STG) impregnated Kevlar fabrics

To cite this article: Chunyu Zhao *et al* 2019 *Smart Mater. Struct.* **28** 075036

View the [article online](#) for updates and enhancements.

Anti-impact behavior of a novel soft body armor based on shear thickening gel (STG) impregnated Kevlar fabrics

Chunyu Zhao¹, Chenhui Xu¹, Saisai Cao¹, Shouhu Xuan^{1,3},
Wanquan Jiang² and Xinglong Gong^{1,3} 

¹ CAS Key Laboratory of Mechanical Behavior and Design of Materials, Department of Modern Mechanics, CAS Center for Excellence in Complex System Mechanics, University of Science and Technology of China, Hefei, Anhui 230027, People's Republic of China

² Department of Chemistry, University of Science and Technology of China, Hefei, Anhui 230026, People's Republic of China

E-mail: xuansh@ustc.edu.cn and gongxl@ustc.edu.cn

Received 22 March 2019, revised 2 May 2019

Accepted for publication 16 May 2019

Published 12 June 2019



CrossMark

Abstract

A novel Kevlar/STG (Kevlar fabrics immersed with shear thickening gel) fabrics composite with high anti-impact performance was fabricated. By utilizing a unique multi-sensor force testing system, both low- and high-velocity impact experiments were conducted to investigate the anti-impact performance of Kevlar/STG fabrics. In low-velocity testing, the attenuation of the impact center force for Kevlar/STG was 64.1%, which was much larger than the Kevlar (27.0%). Under high-velocity loading, the impact force of Kevlar/STG attenuated from 805 N to 223 N with the increase of layers from 5-layers to 20-layers, while they reduced from 1125 N to 460 N for Kevlar fabrics. Meanwhile, the failure mode was analyzed and it was found that the high anti-impact performance was originated from the shear thickening effect and enhanced friction. In consideration of the good flexibility and excellent safe guarding property, the Kevlar/STG showed promising perspective in body armor.

Supplementary material for this article is available [online](#)

Keywords: fabrics, smart materials, impact behavior, shear thickening

(Some figures may appear in colour only in the online journal)

1. Introduction

Because of the frequent regional conflicts, the development of innovative safe-guarding materials toward body armor has attracted increasing attention of researchers all over the world. Actually, most of the previous protecting materials were composed of hard substrates, such as metal [1], aluminium alloy [2], and high-strength ceramic/metal composites [3], silicon nitride ceramics [4], etc. To improve the flexibility, soft fiber-reinforced materials [5, 6] with considerable light weight became attractive. Recently, due to the low density, high strength and ease of processing, high-strength flexible

protective materials such as Kevlar fabrics [7, 8] have been intensively investigated. To enlarge their application in soft body armor, various methods were developed to strengthen the Kevlar fabrics by remoulding the structure or changing composition.

It was found that the friction between the Kevlar fabrics played a very important role in enhancing the ballistic resistance [9, 10]. Since the smooth surface fabrics often weakened their energy absorption behavior during the impact process, many efforts have been done to increase the friction between Kevlar fabrics. Sun *et al* [11] modified the Kevlar surface with non-polymerized plasma gas N₂ and chemical vapor (CH₃)₂Cl₂Si to improve the friction of the fabrics. Moreover, high-molecular polymer [12], nanoparticle [13]

³ Authors to whom any correspondence should be addressed.

Table 1. The parameters of Kevlar and Kevlar/STG.

Sample	Layers	Mass (g)	Content of STG (wt%)	Areal Density ($\text{kg} \cdot \text{m}^{-2}$)	Thickness (mm)
Kevlar	5	10.00	0	1.000	1.38
	10	20.00	0	2.000	2.60
	15	30.00	0	3.000	3.90
	20	40.00	0	4.000	5.50
Kevlar/STG	5	18.42	45.81	1.842	1.80
	10	38.69	48.46	3.869	3.80
	15	59.24	50.24	5.924	5.61
	20	79.59	50.39	7.959	7.37

and graphene material [14] could be added into the gaps between Kevlar fabrics by immersion method to prepare high performance Kevlar composites with enhanced friction. Both the experiments and simulations illustrated that the anti-impact performance of Kevlar was effectively improved after surface treatment [15].

Shear thickening, of which the viscosity raised apparently as the shear rate increased [16], was a common physical phenomenon in concentration suspensions. Originated from this wonderful effect, the shear thickening fluids (STF) could reasonably strengthen the Kevlar fabrics. After Lee firstly developed the STF/Kevlar [17], the as-named fluidic body armor attracted increasing interests in anti-impact equipment. The detailed anti-impact mechanism of the STF/Kevlar has been intensively studied and it was found that the mechanical properties of the STF directly affected the final improving performance. The quasi-static testing [18, 19] and high strain rate Split-Hopkinson pressure bar (SHPB) tests [20] indicated that the anti-impact properties of the multi-layers Kevlar fabrics were increased due to the synergistic effect between the surface friction-enhancement and shear thickening behavior. However, since the fluidic nature and long-time instability, the STF encountered the sealing problem when it was impregnated into the Kevlar fabrics. To this end, developing novel shear thickening materials for strengthening Kevlar fabrics became an urgent task.

To our knowledge, the mechanical property such as the shear storage modulus of many polymers increased with the shear frequency. Typically, the shear thickening gel (STG), a high molecular polymer, showed a shear stiffening effect similar to the STF [21, 22]. By applying a sudden external loading, the plastic STG rapidly transformed from the viscous state to elastic materials. Due to the broken-and-recoverable B–O ligand interaction [23], the STG could dissipate impact energy at high strain rate. Many research showed that the STG could be well combined with other enhancing particles to achieve advanced protecting performance [24, 25] and further broadened magnetorheological properties of composites [26–28] by introducing magnetic-particle into STG structure [29]. However, the detailed strengthening mechanism of STG on the Kevlar fabrics has not been clearly claimed until now. In consideration of the broad potential of STG in energy adsorption [30], the construction of STG impregnated Kevlar composite (Kevlar/STG) toward a novel soft body armor was very significant.

**Figure 1.** The schematic of the dissolution-volatilization fabrication procedure to prepare Kevlar/STG composites.

In this work, the high performance safe-guarding composite composed of STG impregnated Kevlar fabrics was developed by solution dissolution-volatilization method. To investigate the energy adsorption behavior, both low-velocity drop tower and high-velocity ballistic impact experiments were conducted. The yarn pull-out testing proved the friction enhancement effect of STG after immersion in Kevlar. Therefore, the Kevlar/STG composite exhibited excellent impact attenuation and energy dispersion. A multi-sensor force testing system was designed to analyze the anti-impact mechanism of the Kevlar/STG. Based on the experiments and discussions, the Kevlar/STG composite was considered to have excellent application as a soft wearable protective material.

2. Materials and methods

2.1. Materials and preparation

Boric acid, dimethyl silicone oil, ethanol, benzoyl peroxide (BPO) (Sinopharm Chemical Reagent Co. Ltd, Shanghai, China) were raw materials to synthesize STG. Acetone (Sinopharm Chemical Reagent Co. Ltd, Shanghai, China) was the solvent to dissolve the STG. Kevlar fabrics (Junantai Protection Technologies Co. Ltd, Beijing, China) were a type of plain-woven high-performance aramid.

Firstly, the boric acid was heated at 160 °C in the oven for 2 h to gain pyroboric acid. Then, pyroboric acid, dimethyl silicone oil (mass ratio 2:15) and ethanol were mixed in a beaker and heated for 7 h at 240 °C to obtain the raw STG

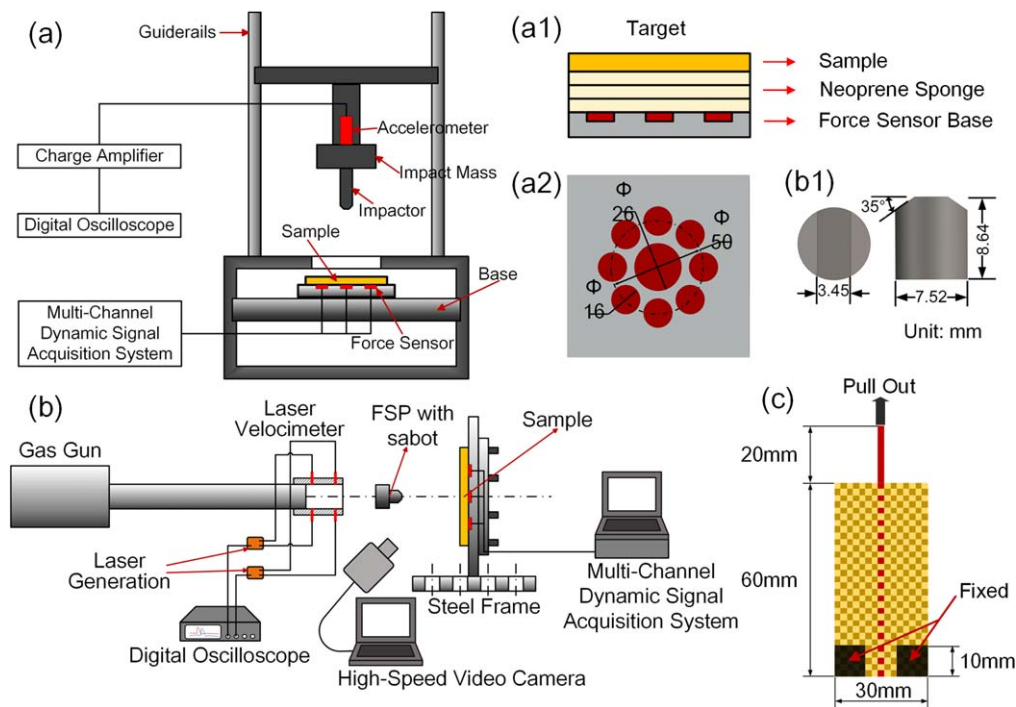


Figure 2. (a) The schematic of the drop tower test device for low velocity impact testing: (a1) the target consisting of composites, the backing material and the force sensor base, (a2) the positions of force sensors; (b) The schematic of the ballistic impact testing system: (b1) dimensions of the FSP; (c) The schematic of the yarn pull-out testing.

polymer. Subsequently, the raw STG polymer colloid and BPO (mass ratio 1:25) were completely dissolved in the acetone. Afterward, the STG solution with a concentration of 0.2 g ml^{-1} was incorporated into the Kevlar fabrics ($10 \text{ cm} \times 10 \text{ cm}$, with an area density of $200 \text{ g} \cdot \text{m}^{-2}$). In this way, the STG solution uniformly filled into the gaps between the surface and the layers of fabrics through solution osmosis and the infiltration STG mass could be accurately controlled. With the volatility of the acetone in the 50°C oven, 2 g STG could adhere to the Kevlar fabrics. At last, multi-layers Kevlar/STG composite (figure 1) was produced by repeating the abovementioned dissolution-volatilization progress, and the content of STG was almost 50 wt%. For simplicity, the multi-layers Kevlar fabrics were defined as ‘X layer Kevlar’ and the multi-layers Kevlar/STG composites were defined as ‘X layer Kevlar/STG’. X was the number of layers. In this experiment, X was 5, 10, 15 and 20, respectively. The areal density of 20 layer Kevlar was almost the same to the areal density of 10 layer Kevlar/STG. The specific parameters of the Kevlar/STG composites were shown in table 1.

2.2. Low-velocity drop tower impact testing

Low-velocity impact drop tower testing system (figure 2(a)) consisted of a drop tower test device (ZCJ1302-A, MTS Co. Ltd, China), an acceleration sensor, force sensors, and a dynamic signal test and analysis system (DH5920N, Donghua Testing Technology Co., Ltd, Jiangsu, China). The impact target was made up of the force sensor base, sample, and a 2 cm neoprene sponge layer (figure 2(a1)). A 1.97 kg impactor

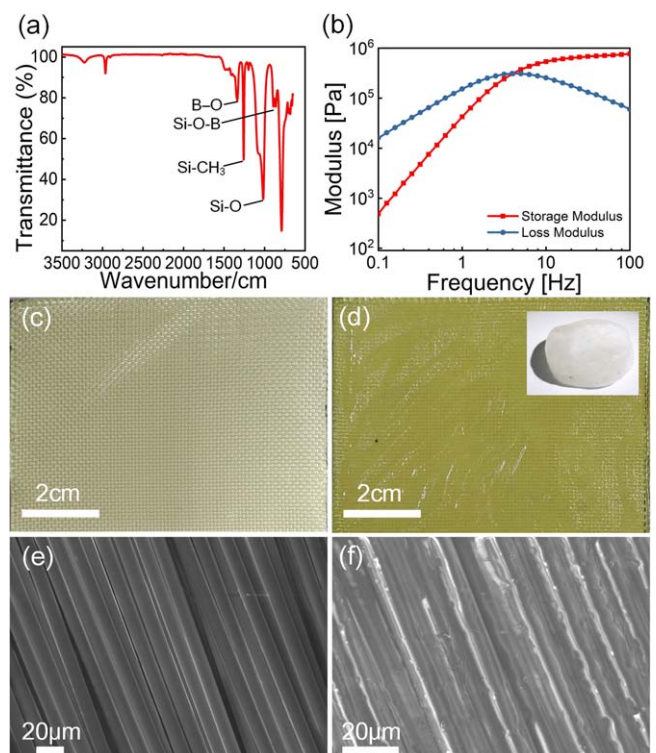


Figure 3. (a) The FTIR spectrum of the STG in the range of $3500\text{--}500 \text{ cm}^{-1}$; (b) The curves of storage modulus and loss modulus versus shear frequency of STG; (c) The macroscopic images of (c) neat Kevlar and (d) the Kevlar/STG (inset image is the steady state of STG); The microscopic SEM images of (e) neat Kevlar and (f) Kevlar/STG.

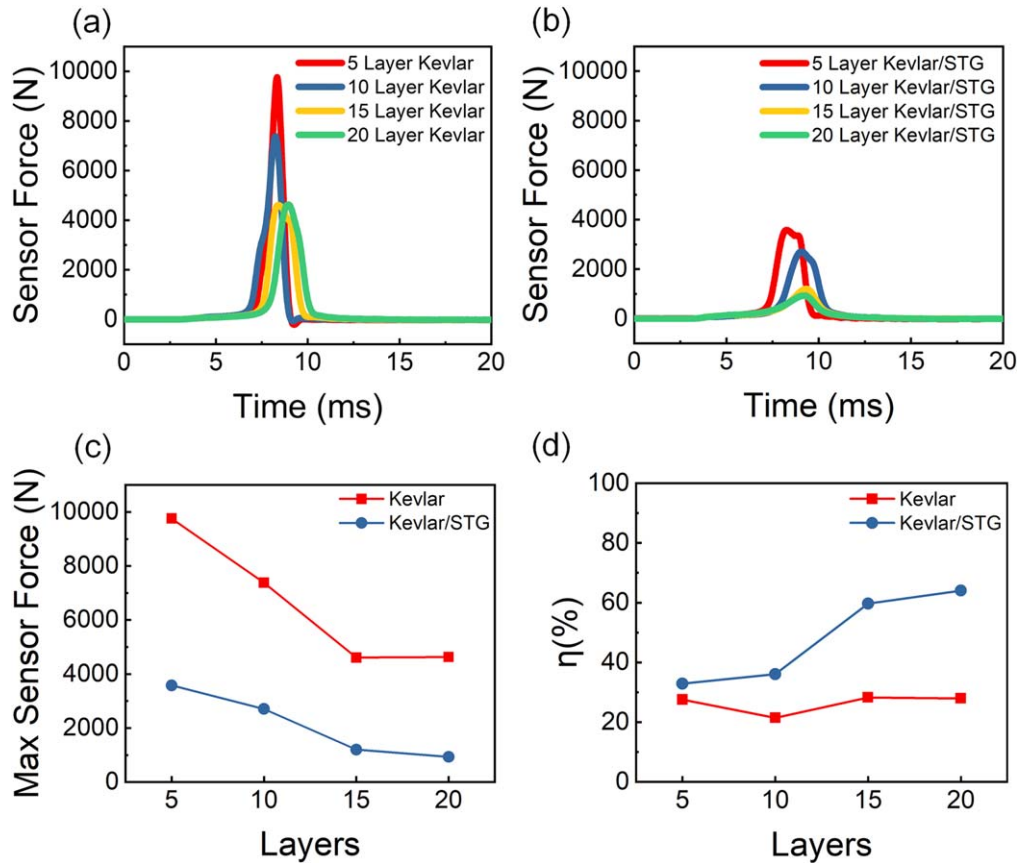


Figure 4. Low-velocity impact: the curve of center impact force versus time for (a) different layers neat Kevlar and (b) different layers of Kevlar/STG composite; (c) The maximum center impact force and (d) center impact force loss of different samples.

dropped from a height of 1 m to impact the target. The impactor had the same shape and dimension as the fragment simulating projectiles (FSP), except for the length. During the impact, the acceleration sensor collected the acceleration signals of the drop tower on the impact surface. Meanwhile, there were 9 force sensors distributed in the target (figure 2(a2)) to collect the force signals loading on the backing material. Under the impact load, the force of different regions could be obtained and compared, which helped to better analyze the complete force information during the impact process. The force signals during the impact process were recorded simultaneously by the dynamic signal test and analysis system. Particularly, the target was fixed by the latex rubber rings and the boundary condition was free.

2.3. High-velocity ballistic impact testing

The high-velocity ballistic impact testing experimental system was set up by using a gas gun as the launcher, a laser velocimeter to measure the impact velocity of the projectile, the projectile with a sabot, the target fixed on a steel frame, a high-speed video camera and the force sensors (figure 2(b)). According to the National Institute of Justice (NIJ) Standard 0101.04, a 44 grain (2.85 g) chisel-nosed steel FSP was used as a projectile (figure 2(b1)). In this testing, the velocity of the projectile was controlled at $103 \pm 8 \text{ m s}^{-1}$. At the same time, the impact force was recorded by the force sensors, the

dynamic signal test, and analysis system. In addition, the high-speed video camera (Phantom v2512, Vision Research Inc.) was adopted to capture the deformation and destruction process of the samples. The target sample was placed approximately 15 cm away from the muzzle so that the yaw and velocity decay of the FSP could be neglected.

2.4. Yarn pull-out testing

The yarn pull-out testing was conducted on MTS CriterionTM Model 43 tensile testing machine. As shown in figure 2(c), the size of the sample was 30 mm × 60 mm. An 80 mm yarn in the middle of the fabrics was used as the pull-out end and the outstretched part of this yarn was fixed by a mobile chuck. The fixed end of the fabric was clamped in the black area of figure 2(c). The middle yarn was pulled out with the movement of the mobile chuck, and the signals of pull-out force and displacement were dynamically collected by the force sensor. In this testing, the velocities of the pull-out end were 50, 400 and 800 mm min^{-1} , respectively.

3. Results and discussion

3.1. Characterization

The Fourier Transform Infrared Spectroscopy (FTIR) technique in a Bruker alpha apparatus was used to investigate the

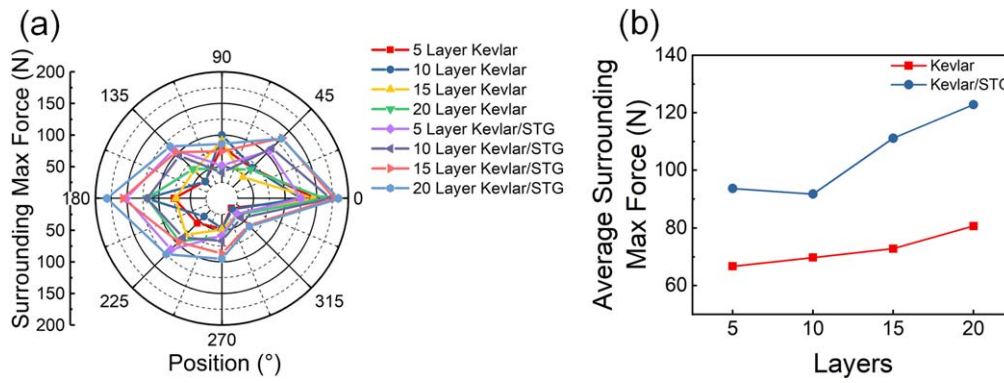


Figure 5. Low-velocity impact: (a) the distribution of the surrounding maximum force and (b) the average surrounding maximum force of the different layers of Kevlar and Kevlar/STG.

chemical characteristic of the STG through ATR mode from 3500 to 500 cm^{-1} (figure 3(a)). The IR spectra performance of STG were obtained by the stretching vibrations of Si-CH₃ group (1257 cm^{-1}), Si-O bond (1015 cm^{-1}) and Si-O-B (892 cm^{-1} and 862 cm^{-1}). Moreover, the previous researches [31] indicated that the B-O bonds at 1336 cm^{-1} could dissipate a large quantity of energy through the unique breaking and reformation behavior.

Rheological property of STG was investigated by using a rheometer (Physica MCR 302, Anton Paar Co., Austria) under the frequency ranging from 0.1 Hz to 100 Hz. The continuous curve of storage modulus and loss modulus versus frequency (figure 3(b)) displayed the shear thickening performance of STG. It was shown that the storage modulus of STG increased with the improving frequency. While for loss modulus, at low frequency (0.1–1.3 Hz), it exhibited an increasing behavior. When the frequency increased from 1.3 to 100 Hz, the loss modulus decreased. This result indicated that the STG possessed perfect shear thickening property and it transformed into a solid-like state at the high shear frequency.

An ordinary digital camera and SEM (FEI XL-30ESEM) were used to investigate the macroscopic (figures 3(c), (d)) and microscopic (figures 3(e), (f)) morphologies of Kevlar and Kevlar/STG. The color of Kevlar/STG changed to bright yellow after combining with STG which illustrated that the STG evenly covered on the surface of Kevlar. Before immersing treatment, many gaps between the Kevlar fabrics could be observed in the neat Kevlar (figure 3(e)). Owing to fluidic characteristic under the quasi-static state, these gaps were completely filled by STG (figure 3(f)).

3.2. Low-velocity drop tower impact testing

In the low-velocity impact testing, the curve of impact force in the center position (F_c) versus time reflected the anti-impact effect of samples (figures 4(a), (b)). Obviously, F_c was affected by layers and composition. With the increasing of the layer number, the maximum center impact force ($F_{c-\max}$) of neat Kevlar decreased from 9759 N (5 layers) to 4630 N (20 layers) (figure 4(c)). While the $F_{c-\max}$ of Kevlar/STG only decreased from 3579 N (5 layers) to 930 N (20 layers). The $F_{c-\max}$ of Kevlar/STG was 2–4 times lower than the same

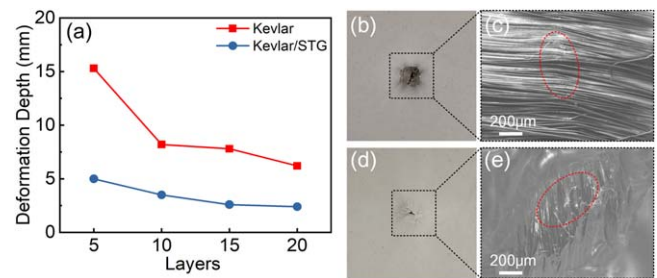


Figure 6. Low-velocity impact: (a) the sinking depth and backing of 5, 10, 15 and 20 layer Kevlar and Kevlar/STG composite; (b) The backing material destruction morphology of 5 layer neat Kevlar; (c) Destruction morphology of neat Kevlar after low-velocity impact; (d) The backing material destruction morphology of 5 layer Kevlar/STG; (e) Destruction morphology of neat Kevlar/STG after low-velocity impact.

layer of Kevlar, displaying a better anti-impact performance than the neat Kevlar fabrics. Importantly, with the same areal density, $F_{c-\max}$ of 10 layer Kevlar and 5 layer Kevlar/STG was 7381 N and 3779 N, and $F_{c-\max}$ of 20 layer Kevlar and 10 layer Kevlar/STG was 4630 N and 2704 N. Hence, the safeguarding property of the Kevlar/STG was better than the multi-layers Kevlar. Because of the excellent shear thickening effect, the Kevlar/STG could effectively decrease the thickness of the samples while keeping the safe-guarding performance. Based on the above results, it could be concluded that the combination of the STG and Kevlar was a reasonable method to develop high performance body armor.

In order to quantify the attenuation effect, the impact force of the drop tower was calculated by the acceleration signal (equation (1)) and the attenuation coefficient of the impact force was obtained by (equation (2)).

$$F_i = ma + mg \quad (1)$$

$$\eta = \frac{F_{c-\max}}{F_{i-\max}} \quad (2)$$

where, F_i was the impact force, m was the mass of the drop tower (1.97 kg), a was the acceleration signal, and g was the gravity acceleration (10 $\text{m} \cdot \text{s}^{-2}$), $F_{c-\max}$ was the maximum sensor force in the center position, $F_{i-\max}$ was the maximum impact force and η was the attenuation coefficient. The

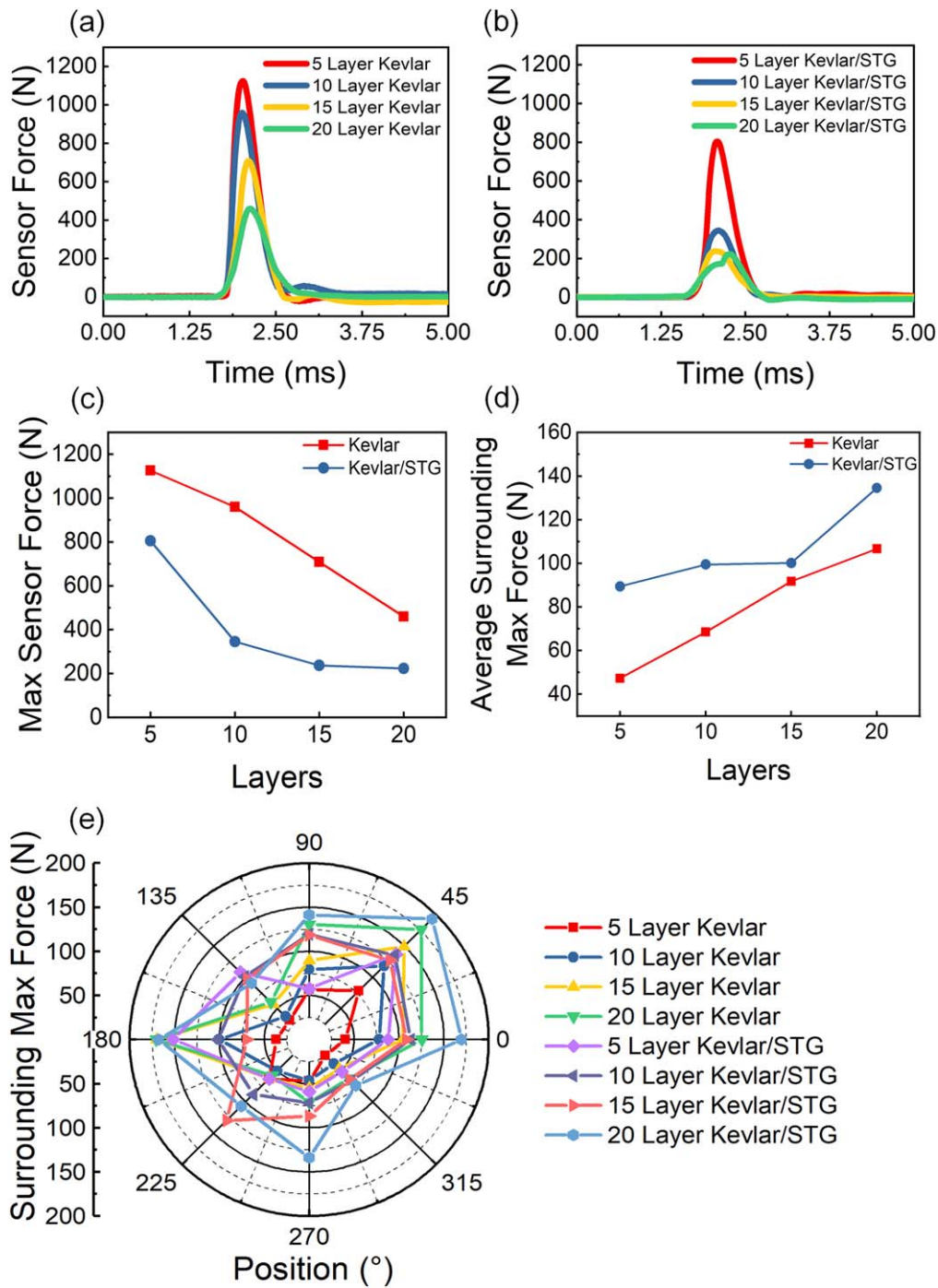


Figure 7. High-velocity ballistic impact testing: the curves of center impact force versus time of (a) neat Kevlar and (b) Kevlar/STG composites; (c) the maximum center impact force and (d) center impact force loss of different samples; (e) the distribution of the surrounding maximum force.

relationship between the attenuation coefficient η and the layers was shown in figure 4(d). The η of 5, 10, 15 and 20 layer Kevlar/STG were 32.9%, 36.1%, 59.7% and 64.1%, which increased with the layer number. However, the η of the neat Kevlar with different layers kept almost the same at around 27.0%. Therefore, the attenuation of the impact force in the center area with the increasing layers was due to the mass increment of STG rather than the Kevlar layers.

To investigate the distribution of the impact force, a multi-sensor force testing system, in which a force sensor was located in the center and 8 force sensors distributed on the circle (25 mm from the center), was designed for both neat Kevlar and Kevlar/STG. Figure 5(a) showed the surrounding maximum force (F_{s-max}) signals, and the distribution of F_{s-max} was not axisymmetric but was like the ‘spindle’ shape. During the impact process, the projectiles

could not accurately contact the sample in the very center area due to the unavoidable differences. Hence, this phenomenon must be responded for the impact of position errors and component dis-homogeneity.

The attenuation effect of the fabrics samples could be discerned according to the area enclosed by the curves. It was found that the force attenuation of 5, 10, 15 and 20 layer Kevlar was smaller than that of Kevlar/STG (figure 5(a)), which illustrated that the Kevlar/STG fabrics possessed a better force attenuation against external impact. Analogously, the Kevlar/STG composite with fewer layers manifested better force attenuation effect than the multi-layer Kevlar. The average value of F_{s-max} for each specimen $\overline{F_{s-max}}$ was also calculated in figure 5(b).

For 5, 10, 15 and 20 layer Kevlar/STG, the minimum value of $\overline{F_{s-max}}$ was 92 N. However, for Kevlar, the maximum value was only 81 N. It was worth mentioning that the backing force of materials in the impact center decreased effectively while the one in the surrounding area increased inversely with the increase of layers. Based on the above analysis, it could be concluded that the force attenuation effect of the Kevlar in the impact surrounding area could be effectively improved by increasing the layer number as well as the introduction of STG.

The anti-impact effect of each sample could be studied through observing the surface deformation and the destruction of the backing material. The obvious perforation in the backing material of 5 layer Kevlar resulted from the impactor penetrating the backing material was observed in figure 6(a). With the increasing layers of Kevlar, the backing material destruction became less obvious. Meanwhile, the sinking depth was also markedly decreased. Specifically, the sinking depth of 5 layer Kevlar/STG composite was less than that of 20 layer Kevlar. Apparently, with the increase of the Kevlar/STG layers, the sinking depth decreased from 5 mm to 2.6 mm and 2.4 mm, while the layers of Kevlar/STG increased from 5 to 15 and 20.

Figures 6(c) and (e) showed the SEM images of the Kevlar and Kevlar/STG fabrics after destruction. Only a slight crease could be observed in Kevlar fabrics while apparent rupture failure occurred in the Kevlar/STG fabrics. During the low-velocity impact testing, Kevlar had enough time to dissipate the impact loading by the deformation of the fabrics. Hence, the impactor could easily penetrate the backing material and generated destruction (figure 6(b)). In this case, the friction of the fabrics was the main form to resist the impact loading. Most of the impact energy could be attenuated and absorbed by backing material, resulting in a worse anti-impact effect and large fabrics deformation. Oppositely, the flexural rigidity of Kevlar/STG was significantly improved and the bending deflection of fabrics played a significant role in resisting against the impact. To this end, the deformation during the impact process was resisted. Due to the tight adhesion between fabrics and STG, energy absorption was increased. Thus, the impact energy acted on the backing material was drastically reduced (figure 6(d)). Therefore, the destruction morphology of neat Kevlar fabrics was not easy to be observed while the Kevlar/STG was much clearer.

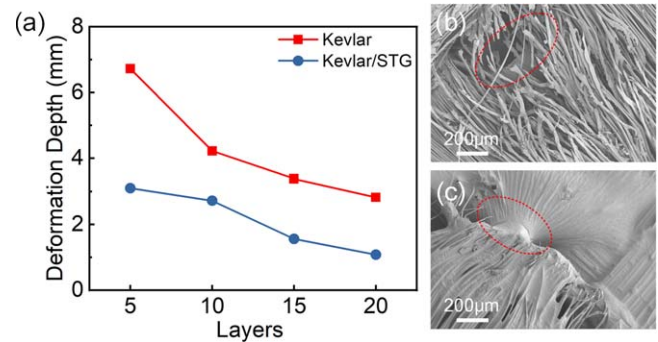


Figure 8. High-velocity ballistic impact testing: (a) the sinking depth and backing material of 5, 10, 15 and 20 layer Kevlar and Kevlar/STG composite; (b) Kevlar fabrics destruction morphology; (c) Kevlar/STG fabrics destruction morphology.

3.3. High-velocity ballistic impact

Similarly, in ballistic impact testing, the impact force in the center position (F_c) versus time reflected the high-velocity anti-impact effect (figures 7(a), (b)). With increasing of the layers number, the F_{c-max} of Kevlar evenly decreased from 1125 N (5 layers) to 460 N (20 layers). However, the F_{c-max} of Kevlar/STG decreased rapidly from 805 N (5 layers) to 345 N (10 layers) and then decreased tardily to 233 N (20 layers) (figure 7(c)). In comparison to the neat Kevlar, F_c of Kevlar/STG was much smaller, which declared that the STG decreased the backing force in the impact center during the high-velocity ballistic impact testing. In this work, it was also found that the F_{c-max} of Kevlar/STG composites were lower than the Kevlar fabrics with the same areal density.

The force attenuation behavior also could be investigated to analyze the unique anti-impact of Kevlar/STG (figure 7(e)). Interestingly, with increasing of the layer numbers (from 5 to 20 layer Kevlar/STG), the force attenuation areas were obviously increased, exhibiting a rising anti-impact performance. The largest ability of force attenuation in 20 layer Kevlar/STG demonstrated that the STG exhibited the shear thickening effect in the high shear frequency, which agreed well with the mechanical characteristics of the STG. In order to manifest the attenuation effect of each specimen clearly, $\overline{F_{s-max}}$ was calculated (figure 7(d)). For the samples with the same component, with increasing of the layers, the ability of force attenuation increased and the force in the impact center simultaneously attenuated (figure 7(c)). In consideration of the fracture morphology, the Kevlar/STG possessed better ability to disperse force than Kevlar. Specially, for 20 layer Kevlar/STG, the minimum value of F_{c-max} was only 223N and $\overline{F_{s-max}}$ was 134N. The $\overline{F_{s-max}}$ the value was close to F_{c-max} . As a result, besides keeping flexibility, the high-velocity anti-impact performance of the Kevlar could be effectively improved by introducing STG into the fabrics.

The safeguarding performance of the different layers neat Kevlar and Kevlar/STG was also investigated through analyzing destruction morphology in the backing material. There was obvious deprecation in the backing material of 5 layer Kevlar with the sinking depth of 6.7 mm. With increasing of the Kevlar layers, the destruction of the backing material

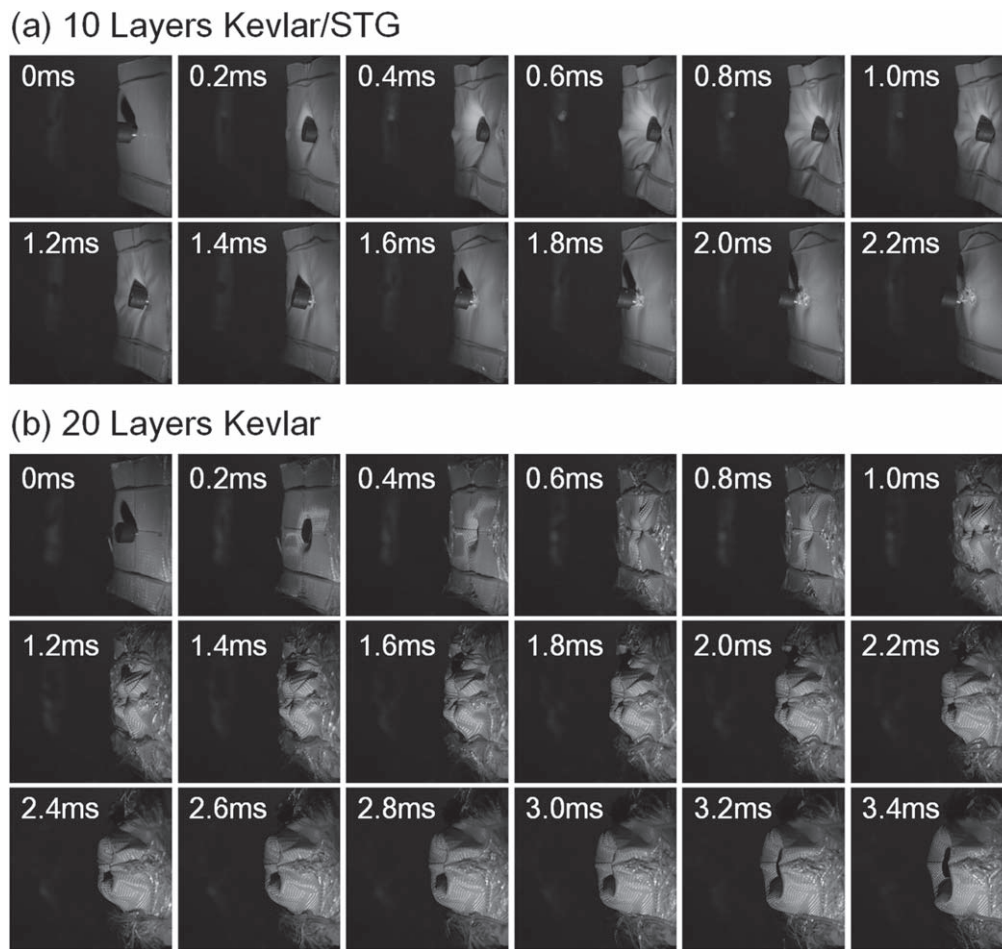


Figure 9. High-velocity ballistic impact testing: (a) the impact process of 10 layer Kevlar/STG and (b) 20 layer Kevlar. The black part was a sabot.

reduced. Specifically, the sinking depth of 20 layer Kevlar decreased to 2.8 mm. Here, the Kevlar/STG showed a smaller depth than the neat Kevlar. When the layer numbers reduced from 20 to 15, 10, and 5, the sinking depth varied from 3.10 to 2.72, 1.56, and 1.08 mm, respectively. These results also illustrated that the Kevlar/STG exhibited better anti-impact performance than the Kevlar fabrics under the high-velocity ballistic impact (Figures 8(a)).

Figures 8(b) and (c) showed the SEM images of the destruction Kevlar and Kevlar/STG fabrics after the ballistic impact. In high-velocity ballistic impact testing, the fabrics breakage was the main failure form. Therefore, for neat Kevlar fabrics, only fabrics breakage could dissipate the impact energy. But for Kevlar/STG with higher flexural rigidity, it could resist deformation more effectively and dissipate impact force to surrounding area concurrently. In this case, the impact of energy could be absorbed effectively in the Kevlar/STG fabrics.

The high-speed video camera was used to capture the deformation and destruction process of the Kevlar (figure 9(a)), movie S1 is available online at stacks.iop.org/SMS/28/075036/mmedia and Kevlar/STG fabrics (figure 9(b)), movie S2). The 10 layer Kevlar/STG and 20 layer Kevlar were taken as examples due to they had the same areal density.

When the FSP impacted the Kevlar/STG, only a slight deformation was found in the target due to its high flexural rigidity and strong interlamination adhesive stress. However, when the FSP contacted the neat Kevlar fabrics, the FSP not only caused large deformation but also penetrated into the soft Kevlar. Moreover, during the rebounding process, the Kevlar was in smooth interlamination status without other constraining force. Then, the deformation occurred easily and caused a kind of ‘crater’ morphology. Obviously, the different deformation morphologies formed the impact process also demonstrated that the anti-impact ability of Kevlar/STG was better than the Kevlar.

3.4. Yarn pull-out testing

It was believed that the better energy dissipation of the Kevlar/STG was partly originated from the enhanced friction between the STG colloid and Kevlar fabrics. Therefore, the yarn pull-out testing was conducted to investigate the detailed mechanism. During the testing, the pull-out force versus the displacement of the pull-out end was collected by the MTS Criterion™ Model 43 (figures 10(a), (c)). An obvious three-state process could be found in pull-out testing. Firstly, the initial state of the pull-out yarn was slack. Once the yarn

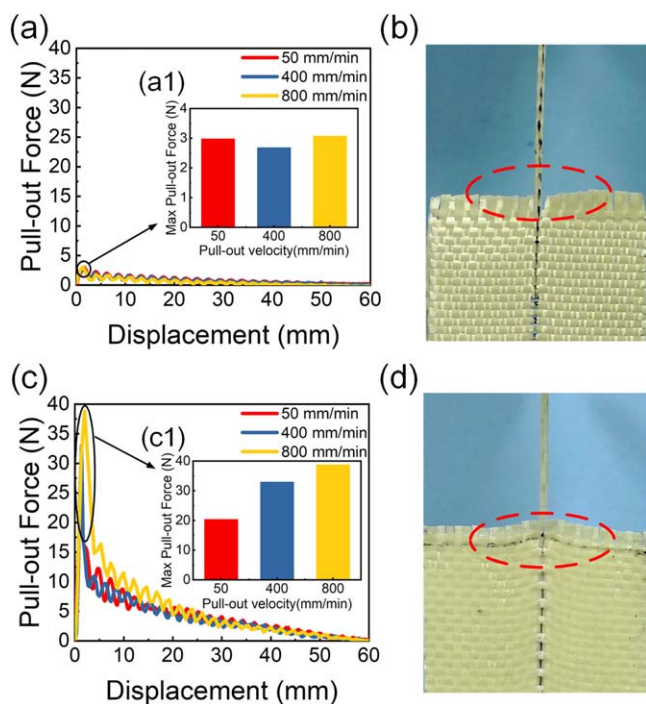


Figure 10. The curve of the pull-out force of single fabrics in the center position with time: (a) monolayer of Kevlar; (c) monolayer of Kevlar/STG; The maximum of the pull-out force of single fabrics in the center position: (a1) monolayer of Kevlar; (c1) monolayer of Kevlar/STG; The transverse deformation of the single fabrics during the pull-out testing: (b) monolayer of Kevlar; (d) monolayer of Kevlar/STG.

started to be pulled out, the pull-out force increased sharply to a maximum value. Secondly, the force declined with fluctuation due to the increase in the length of the yarn being pulled out. The residual crimp in the fabrics led to the transverse vibration of the fabrics which eventually induced the fluctuation of pull-out force. Finally, the yarns were pulled out completely and the pull-out force reduced to 0 N. The Kevlar/STG composite was under a combining state before the pull-out testing. Therefore, it was hard for the yarn to be pulled out in the first stage of the testing. Then, once the yarn started to move, the combined state of the sample was broken which resulted in the rapid decrease of pull-out force.

To further understand the differences of friction between the Kevlar/STG and Kevlar, the maximum pull-out force of the monolayer Kevlar and Kevlar/STG at the pull-out velocities of 50, 400 and 800 mm min⁻¹ (figures 10(a), (c1)) were also compared. For the neat Kevlar, the maximum value of pull-out force (F_{p-max}) almost remained constantly at different pull-out velocities. Nevertheless, for Kevlar/STG, the F_{p-max} increased from 17.0 N, 24.4 N to 29.9 N when the pull-out velocity increased. The STG could not only increase the friction of the fabrics, but also transform the composite into a smart material with the strain-rate dependent mechanical property which meant the friction of the fabrics was also enhanced by the pull-out velocity. During the pulled out process, the fibers around pull-out yarn could transmit load due to the intraformational friction, and then the deformation was generated. The more fabrics area involved in deformation, the more resistance occurred to resist the deformation.

In this work, the deformation of transverse fabrics was recorded by an ordinary camera during the pull-out testing process. It was observed that during the pulling out process, the deformation of transverse fabrics could be hardly discovered (figure 10(b)), which indicated that the loading was not effectively transmitted to the around fabrics. Therefore, the friction resistance against the yarn by pulling out was very small (figure 10(a)). However, for Kevlar/STG (figure 10(d)), larger deformation was found during the pull-out process, which illustrated that STG improved the contact stress of the pull-out fabrics and surrounding fabrics meanwhile increased the friction between the fabrics (figure 10(c)).

3.5. Anti-impact mechanism of the Kevlar/STG

Here, the anti-impact performance of the STG on the Kevlar was also systematically analyzed. The STG had very good shear thickening property and its storage modulus rapidly increased with shear rate. Firstly, the improving protective property of Kevlar/STG was benefited from the shear thickening effect. On the other hand, in comparison to neat Kevlar, the gaps between the fabrics were fulfilled STG (figure 3(f)). When the relative deformation of fabrics generated, the adhesive force between the STG and the fabrics increased the internal friction, which further strengthened the anti-impact property of Kevlar/STG.

During the low-velocity drop tower testing, the friction between the fabrics was the main mode to resist the failure. Without the addition of STG, the yarns of neat Kevlar fabrics were very smooth with gaps so that the friction between the yarns was very small. Therefore, upon the impact, when deformation was generated on the surface of neat Kevlar, an obvious deformation in the impact center was found and the surrounding fabrics were forced to produce wrinkles to prevent penetration (figure 11(a)). In this mode, the friction of fabrics was very limited and the deformation of fabrics was irreversible. However, the Kevlar/STG had better adhesion stress between the fabrics. Due to the presence of STG, it was hard for the fabrics to get relative deformation during the impact process. The increasing internal friction decreased the deformation of fabrics (figure 11(b)). Under this circumstance, more impact energy was dissipated during the impact process and the force sensors under the backing material received weaker force signals.

Moreover, the shear thickening effect in STG was reversible. It was well-known that STG possessed a large number of 'B-O dynamic bonds' (yellow dots in the figure 11(e)), of which the O atom in dimethylsiloxane shared its valence electron with the B atom from boric acid and formed weak bonds between the long molecular chains. When a quasi-static force was loaded on the STG, the molecular chain had sufficient time to disentangle and thus exhibited a soft state. Nevertheless, once the external load was at a high rate, the 'B-O dynamic bonds' could not be destroyed in a short time and a stable polymer network was formed. Because of entanglement of the long molecular chains, the STG performed a solid-like state immediately.

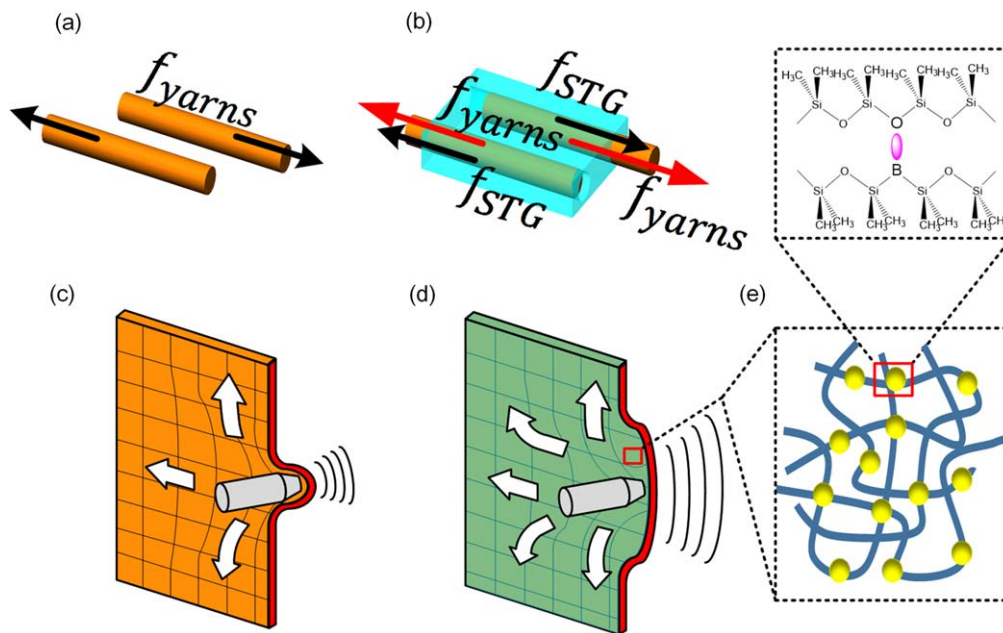


Figure 11. The schematic of the propagation of the transverse stress in the fabrics: Morphology feature of samples during low-velocity ballistic impact: (a) Kevlar fabrics; (b) Kevlar/STG fabrics; Morphology feature of samples after during high-velocity impact testing: (c) Kevlar fabrics; (d) Kevlar/STG fabrics; (e) the microscopic structure of STG and the ‘B–O dynamic bonds’.

In high-velocity ballistic testing, the Kevlar fabrics withstood the penetration of FSP by the breakage of the fabrics and the protecting effect was relatively limited (figure 11(c)). Nevertheless, once the STG was introduced into Kevlar fabrics, the stiffness of Kevlar fabric was enhanced to resist the penetration of FSP during the ballistic impact process. On account of the shear thickening performance, as soon as the FSP touched the fabrics, the STG firstly transformed from plastic to solid state to resist the impact due to the high impact rate (figure 11(d)). During the impact, the impact force was gradually dispersed and weakened. Therefore, a large amount of STG was pulverized into a powder, further led to a large amount of energy dissipation. Then, the fabrics yarns were broken to disperse impact energy again. In this case, not only the anti-impact performance was improved, but also the damage morphology became rarely obvious. Finally, the STG significantly improved anti-impact performance.

4. Conclusion

In this work, a novel Kevlar/STG soft body armor material was prepared by impregnating STG into Kevlar fabrics. The dynamic mechanical testing under low- and high- velocity impact was applied to investigate the safeguarding property of the Kevlar/STG composite. Besides, a multi-sensor target testing system was applied to analyze the impact force, and the distributions of the impact force could be obtained and detailed energy dispersion behavior was illustrated. Due to the shearing thickening property and the increasing friction, the STG could significantly improve the anti-impact performance of the Kevlar fabrics in both low- and high-velocity testing.

Moreover, the destruction morphology of Kevlar/STG was much slighter than the ‘crater’ morphology of Kevlar fabrics. A possible mechanism was proposed to explain the anti-impact performance of Kevlar/STG and detailed effects of STG on the energy dispersion were claimed. Based on the experimental results, it was found that the Kevlar/STG composite with good protection properties possessed a broad application potential in personal body armor.

Acknowledgments

Financial supports from the National Natural Science Foundation of China (Grant No. 11822209, 11772320), the Strategic Priority Research Program of Chinese Academy of Sciences (Grant No. XDB22040502), and the Fundamental Research Funds for the Central Universities (WK2090050045) are gratefully acknowledged. This study was also supported by the Collaborative Innovation Center of Suzhou Nano Science and Technology.

ORCID iDs

Xinglong Gong  <https://orcid.org/0000-0001-6997-9526>

References

- [1] Palleti H, Gurusamy S, Kumar S, Soni R, John B, Vaidya R, Bhoge A and Naik N K 2012 Ballistic impact performance of metallic targets *Mater. Des.* **39** 253–63
- [2] Jha A K, Shiresha N, Murty S, Diwakar V and SreeKumar K 2005 Ballistic impact testing of AA21219 aluminium alloy

- welded plates and their metallurgical characterisation *Indian J. Eng. Mater. Sci.* **12** 221–6
- [3] Tan Z H, Han X, Zhang W and Luo S H 2010 An investigation on failure mechanisms of ceramic/metal armour subjected to the impact of tungsten projectile *Int. J. Impact Eng.* **37** 1162–9
- [4] Kelina I Y and Dobrinskii Y I 1997 Efficiency of the use of silicon nitride ceramics as an armor material *Refract. Ind. Ceram.* **38** 220–3
- [5] Hwang H S, Malakooti M H, Patterson B A and Sodano H A 2015 Increased inter yarn friction through ZnO nanowire arrays grown on aramid fabric *Compos. Sci. Technol.* **107** 75–81
- [6] Wang P F, Yang J L, Liu W S, Tang X Z, Zhao K, Lu X H and Xu S L 2017 Tunable crack propagation behavior in carbon fiber reinforced plastic laminates with polydopamine and graphene oxide treated fibers *Mater. Des.* **113** 68–75
- [7] Monteiro S N, Milanezi T L, Louro L H L, Lima E P, Braga F O, Gomes A V and Drelich J W 2016 Novel ballistic ramie fabric composite competing with KevlarTM fabric in multilayered armor *Mater. Des.* **96** 263–9
- [8] Bandaru A K, Chavan V V, Ahmad S, Alagirusamy R and Bhatnagar N 2016 Ballistic impact response of Kevlar[®] reinforced thermoplastic composite armors *Int. J. Impact Eng.* **89** 1–13
- [9] Park Y, Kim Y, Baluch A H and Kim C G 2015 Numerical simulation and empirical comparison of the high velocity impact of STF impregnated Kevlar fabric using friction effects *Compos. Struct.* **125** 520–9
- [10] LaBare E D, Calderon-Colon X, Morris M, Tiffany J, Wetzel E, Merkle A and Trexler M 2015 Effect of a carbon nanotube coating on friction and impact performance of Kevlar *J. Mater. Sci.* **50** 5431–42
- [11] Sun D M and Chen X G 2012 Plasma modification of Kevlar fabrics for ballistic applications *Text. Res. J.* **82** 1928–34
- [12] Lin T K, Wu S J, Lai J G and Shyu S S 2000 The effect of chemical treatment on reinforcement/matrix interaction in Kevlar-fiber/bismaleimide composites *Compos. Sci. Technol.* **60** 1873–8
- [13] Liu N, Wang J Z, Yang J, Han G F and Yan F Y 2016 Combined effect of nano-SiO₂ and nano-Al₂O₃ on improving the tribological properties of Kevlar fabric/phenolic laminate in water *Tribol. Trans.* **59** 163–9
- [14] Tan Z H, Li W H and Huang W 2018 The effect of graphene on the yarn pull-out force and ballistic performance of Kevlar fabrics impregnated with shear thickening fluids *Smart Mater. Struct.* **27** 075048
- [15] Mishra R, Behera B K and Militky J 2016 Impact simulation of three-dimensional woven kevlar-epoxy composites *J. Ind. Text.* **45** 978–94
- [16] Tian T F, Li W H, Ding J, Alici G and Du H 2012 Study of shear-stiffened elastomers *Smart Mater. Struct.* **21** 125009
- [17] Lee Y S, Wetzel E D and Wagner N J 2003 The ballistic impact characteristics of Kevlar (R) woven fabrics impregnated with a colloidal shear thickening fluid *J. Mater. Sci.* **38** 2825–33
- [18] Feng X Y, Li S K, Wang Y, Wang Y C and Liu J X 2014 Effects of different silica particles on quasi-static stab resistant properties of fabrics impregnated with shear thickening fluids *Mater. Des.* **64** 456–61
- [19] Lu Z Q, Jing X Y, Sun B Z and Gu B H 2013 Compressive behaviors of warp-knitted spacer fabrics impregnated with shear thickening fluid *Compos. Sci. Technol.* **88** 184–9
- [20] Cao S S, Chen Q, Wang Y P, Xuan S H, Jiang W Q and Gong X L 2017 High strain-rate dynamic mechanical properties of Kevlar fabrics impregnated with shear thickening fluid *Compos. Part A-Appl. S* **100** 161–9
- [21] Martin R, Rekondo A, de Luzuriaga A R, Santamaria A and Odriozola I 2015 Mixing the immiscible: blends of dynamic polymer networks *RSC Adv.* **5** 17514–8
- [22] Rudolf M, Boutelier D, Rosenau M, Schreurs G and Oncken O 2016 Rheological benchmark of silicone oils used for analog modeling of short-and long-term lithospheric deformation *Tectonophysics* **684** 12–22
- [23] Seetapan N, Fuongfuchai A, Sirikittikul D and Limparyoon N 2013 Unimodal and bimodal networks of physically crosslinked polyborodimethylsiloxane: viscoelastic and equibiaxial extension behaviors *J. Polym. Res.* **20** 183
- [24] Zhang S S, Wang S, Wang Y P, Fan X W, Ding L, Xuan S H and Gong X L 2018 Conductive shear thickening gel/polyurethane sponge: a flexible human motion detection sensor with excellent safeguarding performance *Compos. Part A-Appl. S* **112** 197–206
- [25] Wang Y P, Gong X L and Xuan S H 2018 Study of low-velocity impact response of sandwich panels with shear-thickening gel cores *Smart Mater. Struct.* **27** 065008
- [26] Kim W H, Park J H, Kaluvan S, Lee Y S and Choi S B 2017 A novel type of tunable magnetorheological dampers operated by permanent magnets *Sensor. Actuat. A-Phys.* **255** 104–17
- [27] Choi S B, Park Y K and Cheong C C 1996 Active vibration control of intelligent composite laminate structures incorporating an electro-rheological fluid *J. Intell. Mater. Syst. Struct.* **7** 411–9
- [28] Sun S S, Deng H X, Li W H, Du H P, Ni Y Q, Zhang J and Yang J 2013 Improving the critical speeds of high-speed trains using magnetorheological technology *Smart Mater. Struct.* **22** 115012
- [29] Wang Y P, Wang S, Xu C H, Xuan S H, Jiang W Q and Gong X L 2016 Dynamic behavior of magnetically responsive shear-stiffening gel under high strain rate *Compos. Sci. Technol.* **127** 169–76
- [30] Deng H X, Du Y, Wang Z M, Ye J C, Zhang J, Ma M C and Zhong X 2019 Poly-stable energy harvesting based on synergetic multistable vibration *Commun. Phys.* **2** 21
- [31] Wang S, Jiang W Q, Jiang W F, Ye F, Mao Y, Xuan S H and Gong X L 2014 Multifunctional polymer composite with excellent shear stiffening performance and magnetorheological effect *J. Mater. Chem. C* **2** 7133–40